

Tidal disruption, global mass function and structural parameters evolution in star clusters

Michele Trenti

*University of Colorado, CASA, Dept. of Astrophysical & Planetary Sciences, 389-UCB,
Boulder, CO 80309, USA*

trenti@colorado.edu

Enrico Vesperini

Department of Physics, Drexel University, Philadelphia, PA 19104, USA

Mario Pasquato

Dipartimento di Fisica, Università di Pisa, Largo Bruno Pontecorvo 3, 56127 Pisa, Italy

ABSTRACT

We present a unified picture for the evolution of star clusters on the two-body relaxation timescale. We use direct N-body simulations of star clusters in a galactic tidal field starting from different multi-mass King models, up to 10% of primordial binaries and up to $N_{tot} = 65536$ particles. An additional run also includes a central Intermediate Mass Black Hole. We find that for the broad range of initial conditions we have studied the stellar mass function of these systems presents a universal evolution which depends only on the fractional mass loss. The structure of the system, as measured by the core to half mass radius ratio, also evolves toward a universal state, which is set by the efficiency of heating on the visible population of stars induced by dynamical interactions in the core of the system. Interactions with dark remnants (white dwarfs, neutron stars and stellar mass black holes) are dominant over the heating induced by a moderate population of primordial binaries (3-5%), especially under the assumption that most of the neutron stars and black holes are retained in the system. All our models without primordial binaries undergo a deep gravothermal collapse in the radial mass profile. However their projected light distribution can be well fitted by medium concentration King models (with parameter $W_0 \sim 8$), even though there tends to be an excess over the best fit for the innermost points of the surface brightness. This excess is consistent with a shallow cusp in the surface brightness ($\mu \sim R^{-\nu}$ with $\nu \sim 0.4 - 0.7$), like it has been observed for many globular clusters

from high-resolution HST imaging. Generally fitting a King profile to derive the structural parameters yields to larger fluctuations in the core size than defining the core as the radius where the surface brightness is one half of its central value. Classification of core-collapsed globular clusters based on their surface brightness profile may thus fail in systems that appear to have already bounced back to lower concentrations, particularly if the angular resolution of the observations is limited and the core is not well resolved.

Subject headings: Stars: luminosity function, mass function – Galaxy: globular clusters: general – Methods: n-body simulations – stellar dynamics

1. Introduction

Until a few years ago, the standard picture of globular clusters stellar population and dynamical evolution emerging from theoretical and observational studies was yielding a consistent and well understood framework. Globular clusters were thought to be ‘simple stellar population’, composed of stars with the same age and chemical composition. Globular cluster dynamical evolution had been thoroughly investigated by a large number of numerical studies showing that clusters surviving the early expansion triggered by primordial gas expulsion and mass loss due to stellar evolution evolve, due mainly to two-body relaxation, toward core collapse and higher central concentrations while losing stars through the boundary set by the tidal field of their host galaxy (see e.g. Heggie & Hut 2003).

In the last few years, however, a wealth of observational data mostly from exquisite space based observations have revealed the actual complexity of globular cluster dynamics and stellar populations. It is now clear that there is a close link and interplay between dynamical evolution and the stellar content of clusters, the structure of clusters and the abundances of exotic objects (such as blue stragglers, X-ray sources, pulsars etc.) (see e.g. Belczynski et al. 2006; Shara & Hurley 2006; Hut 2006).

Recently, a number of photometric and spectroscopic observations have also shown evidence of the presence of multiple stellar populations and challenged the commonly held view according to which globular cluster are ‘simple stellar populations’. It appears that essentially any globular cluster that has high quality photometric and spectroscopic data available presents evidence against a single star-formation burst (Gratton et al. 2004; Bedin et al. 2004; Piotto et al. 2005, 2007; Carretta et al. 2009). The presence of multiple stellar populations has major implications for the formation and the early evolution of globular clusters (see e.g. D’Ercole et al. 2008).

Furthermore, our understanding of the late-time evolution of globular clusters has been called into question. A recent observational study De Marchi et al. (2007), focused on the stellar mass function of Galactic globular clusters, found that clusters with lower concentration index of the surface brightness profile tend to have flatter stellar mass functions. The observed trend is at odds with what is expected from the standard dynamical evolution scenario according to which as clusters evolve toward core collapse and higher concentrations they lose mass and the preferential loss of low-mass stars flattens the stellar mass function; dynamically older clusters should be more centrally concentrated and have flatter stellar mass functions. Baumgardt et al. (2008) have suggested that strong primordial mass segregation might be required to explain the flat stellar mass function of some of the low-concentration cluster in the observed sample of De Marchi et al. (2007). However a strong primordial mass segregation might lead to the rapid dissolution of the cluster due to stellar evolution mass-losses (Vesperini et al. 2009).

High-resolution photometry of the center of globular clusters has also revealed that the standard King (1966) models do not capture the details of the surface brightness profile, which often shows the presence of shallow cusps within a relatively large core (Noyola & Gebhardt 2006). The shallow cusps contrast with the classic expectation that a strong, isothermal cusp develops as a result of core-collapse. The presence of a central IMBH is a possible explanation for the presence of those cusps (Baumgardt et al. 2004; Trenti et al. 2007), but this interpretation appears in contrast with the lack of strong evidence for IMBHs in globular clusters (e.g. see Gill et al. 2008, and references therein). NGC2298, for example, is one of the clusters showing a central excess in the surface brightness profile from the Noyola & Gebhardt (2006) data, but a central IMBH is ruled out at high confidence level (Pasquato et al. 2009).

The goal of this paper is to study in detail the relation between a cluster structural properties and the dynamical phases of its evolutionary path as well as the relation between the properties of a cluster stellar mass function and its structure. We focus our attention on the long-term evolution of star clusters driven by the effects of two-body relaxation. We analyze our numerical models following the procedures used in the observational studies of the structure and stellar content of star clusters and by directly comparing our results with observational data we aim at clarifying their interpretation in the context of dynamic evolution of relaxed stellar systems.

We have carried out a survey of multimass simulations of star clusters evolving in a tidal field and starting from a broad range of different initial conditions spanning different initial density profiles, primordial binary fractions and initial stellar mass function. This paper is organized as follows. In Section 2 we present our sample of simulations. In Section 3 we introduce our framework for analyzing simulations consistently with the observational

derivation of structural quantities. In Section 4 we presents the results of our analysis, concluding in Section 5.

2. Numerical framework

2.1. Past investigations

Numerical investigations of the dynamics of globular clusters are computationally very challenging because of the need to resolve a large dynamic range in timescales, from a few hours typical of a tight binary to the billion of years over which the system evolves due to two-body relaxation. In addition, the computational complexity of a run carried out for a constant number of relaxation times scales as $N^3/\log(N)$, because the relaxation time t_{rh} increases with the number of particles N (e.g see Spitzer 1987). The computational resources required are further increased by the presence of a significant number of binaries, which can be up to 50% of the mass of the core (e.g., see Rubenstein & Bailyn 1997; Albrow et al. 2001; Pulone et al. 2003), although some clusters, like NGC 6397, might also be almost binary-free (Davis et al. 2008). Hard binaries have an important dynamic effect on the evolution of the core size (McMillan et al. 1990, 1991; Vesperini & Chernoff 1994; Heggie, Trenti & Hut 2006). In the past, numerical simulations have been performed either using approximate algorithms such as Monte Carlo methods (e.g., see Gao et al. 1991; Fregeau & Rasio 2007) or direct N-body simulations with a modest number of particles ($N \approx 10^3$ in McMillan et al. 1990 and Heggie & Aarseth 1992) until a recent improvement of one order of magnitude ($N = 16384$ - Heggie, Trenti & Hut 2006; Trenti, Heggie & Hut 2007; Trenti et al. 2007, 2008; Hurley 2007). These investigations highlighted two key results: (i) the presence of a significant population of primordial binaries drives the evolution of the core radius toward a value that is 5 – 10% of the half mass radius and (ii) the ratio of the core to half mass radius (r_c/r_h) does not depend either on its initial value or on the primordial binary fraction f , once a few relaxation times have passed and provided that $f \gtrsim 0.1$. In addition, runs with a galactic tidal field show the central concentration parameter c decreases toward the end of the simulation, due to the combined effect of binaries, that keep a large core, and of the evaporation, that progressively reduces the tidal radius (Trenti, Heggie & Hut 2007). However, the simulations of Trenti, Heggie & Hut (2007) were obtained using simplified initial conditions with equal mass particles and therefore cannot be directly applied to the study of the mass function evolution or analyzed consistently with observations. In this paper we extend our earlier work to include a realistic mass spectrum, as discussed below.

2.2. Our simulations

The simulation framework that we use here has been extensively described in Trenti, Heggie & Hut (2007), Gill et al. (2008) and Pasquato et al. (2009). In short, we follow the evolution of star clusters using the direct summation code NBODY6 (Aarseth 2003), which guarantees an exact treatment of the multiple interactions between stars by employing special regularization techniques, without resorting to the introduction of softening.

Our N-body simulations are carried out in natural (dimensionless) units (Heggie & Mathieu 1986), in which:

$$G = M_T = -4E_T = 1, \quad (1)$$

where M_T is the total mass of the system and E_T the total energy (potential plus kinetic). The corresponding unit of time is:

$$t_d = \frac{(GM_T)^{5/2}}{(4E_T)^{3/2}} = 1, \quad (2)$$

which approximately corresponds to the orbital period at the half-mass radius. In these units, the relaxation time can be written as:

$$t_{rh} = \frac{0.138Nr_h^{3/2}}{\log(0.11N)}, \quad (3)$$

where $r_h \approx 1$ is the radius at which the relaxation time is defined, that is the half-mass radius. Equation 3 can be translated in physical units as follows (Djorgovski 1993):

$$t_{rh} = \frac{8.9 \times 10^5 \text{yr}}{\log(0.11N)} \times \frac{1M_\odot}{\langle m_* \rangle} \times \left(\frac{M_T}{M_\odot} \right)^{1/2} \times \left(\frac{r_h}{1\text{pc}} \right)^{3/2}, \quad (4)$$

where $\langle m_* \rangle$ is the average mass of a star in the system (including dark remnants such as neutron stars).

The individual particle mass is drawn from an initial mass function appropriate to study the late evolutionary stages of star clusters, when stars are $\gtrsim 10$ Gyr old. As in Gill et al. (2008) we consider either a Salpeter (1955) or a Miller & Scalo (1979) initial mass function, that is:

$$\xi(m) \propto m^\alpha, \quad (5)$$

with $\alpha = -2.35$ and $m \in [0.2 : 100]M_\odot$ for the Salpeter IMF, while for the Miller & Scalo IMF the power-law slope is the following: $\alpha = -1.25$ for $m \in [0.2 : 1]M_\odot$, $\alpha = -2.0$ for $m \in [1 : 2]M_\odot$, $\alpha = -2.3$ for $m \in [2 : 10]M_\odot$, and $\alpha = -3.3$ for $m \in [10 : 100]M_\odot$. Before starting the run, an instantaneous step of stellar evolution is taken to evolve the

mass function to a $0.8 M_{\odot}$ turnoff using the Hurley et al. (2000) evolutionary tracks. In our standard models we have a 100% retention fraction of dark remnants. We also run two simulations with a 30% retention fraction of neutron stars and stellar mass black holes (see Table 1). In all simulations no kick velocities are given to the remnants. Our idealized treatment of stellar evolution is based on the approximation that most of the relevant stellar evolution occurs on a timescale shorter than a relaxation time. It is thus appropriate to study the evolution of old globular clusters (age of ~ 10 Gyr). In fact, most of the impact of stellar evolution on the dynamics of a star cluster happens within the first few hundred Myr, when the most massive stars lose a significant fraction of mass and consequently contribute to a global expansion of the system (e.g. see Hurley 2007; Mackey et al. 2008). Later in the life of a star cluster, two-body relaxation tends to erase the memory of the initial density profile and concentration (Trenti, Heggie & Hut 2007; Trenti et al. 2008).

The initial distribution in the position-velocity phase space is that of a King model with scaled central potential $W_0 = 3, 5, 7$. Our standard models have a primordial binary ratio of $f = N_b/(N_s + N_b)$ between 0 and 0.1, with N_s and N_b being the number of singles and binaries respectively. In addition, we also consider a run with a central Intermediate Mass Black Hole (discussed in more detail in Gill et al. 2008). Following Trenti, Heggie & Hut (2007), our initial distribution of the binaries’ binding energies is flat in log scale in the range from ϵ_{min} to $133\epsilon_{min}$, with $\epsilon_{min} = \langle m(0) \rangle \sigma_c(0)^2$. Here $\sigma_c(0)$ is the initial central velocity dispersion and $\langle m(0) \rangle$ is the average stellar mass at $t = 0$. For a typical velocity dispersion $\sigma_c(0) = 10$ km/s, the semi-axes of binaries in the initial conditions are smaller than 10 AU. This choice is motivated by the fact that wider and therefore softer binaries, which are likely created in young star clusters, are destroyed within a few dynamical times and thus would have no effect on the late-time evolution of a star cluster (Heggie 1975). The stellar mass and type of binary members are drawn at random from our initial mass function and thus binaries containing either one or two dark remnants are possible.

The models considered in this paper are tidally limited. The Galactic tidal field is treated as that of a point mass, and the tidal force acting on each particle is computed using a linear approximation of the field. The tidal cutoff radius of the simulation (which we indicate as $\{r_t\}_s$, where the curl-bracket with the suscript “s” is used to denote the definition of a simulation based quantity, see Section 3) is defined as (Spitzer 1987):

$$\{r_t\}_s^3 = \frac{M_T}{3M_{Gal}} R_{Gal}^3, \quad (6)$$

where M_{Gal} is the galaxy mass, and R_{Gal} is the distance of the centre of the star cluster from the centre of the galaxy. We assume R_{Gal} is constant, i.e. the cluster describes a circular orbit. The initial value of $\{r_t\}_s$ is fixed to be self-consistent with the King profile used (for example, the $W_0 = 7$ king model has $\{r_t\}_s = 7.02$ in N-body units). Particles are

removed from the system when they reach a distance $2\{r_t\}_s$ from the center of the cluster (see Trenti, Heggie & Hut 2007 for a full description of the tidal field treatment).

We explore a large parameter space in the initial conditions varying the initial King model concentration, the Roche lobe filling factor, the initial mass function and the primordial binary fraction, as summarized in Table 1. The NBODY6 code has been run with its Graphic Processing Unit extension on the NCSA Lincoln Cluster. Each simulation was assigned to a computing node with 8 cores and two Tesla C1060 GPUs. We measured a sustained computational performance above 0.5 Tflops for a single node, that allowed us to simulate systems with up to $N = 65536$ (or $N = 64\text{k}$ in a compact notation where $1\text{k} \equiv 1024$) particles until either $t = 8000$ was reached (corresponding to several initial relaxation times — $t > 16 t_{rh}(0)$) or at least $\sim 80\%$ of the initial mass is lost due to evaporation of stars.

3. Structural parameters of globular clusters: definitions in simulations and observations

Both space-based photometry with HST and adaptive optics from the ground have greatly improved our knowledge of Galactic globular clusters. In fact, the angular resolution currently available is such that it is possible to resolve faint individual main sequence stars at the center of most Galactic globulars. One of the most striking examples is the globular clusters NGC 2298, where HST photometry reaches a completeness greater than 50% for $0.2 M_\odot$ at the center of the system (De Marchi & Pulone 2007; Pasquato et al. 2009).

A large fraction of globular clusters have been observed with HST (e.g. see Sarajedini et al. 2007), thus acquiring detailed information on their current stellar mass function and their central surface brightness profiles. Here we discuss the definition and determination of structural parameters in both simulations and observations, with the goal to present a consistent analysis of our numerical investigation. Typically, structural properties in numerical simulations are based on a complete knowledge of the system with a tri-dimensional mass-based approach (e.g. the 3D half-mass radius of the system). Observations rely instead on projected two-dimensional data, that are light based (e.g. the 2D half-light radius). In addition, observations are affected by finite angular resolution, limited signal-to-noise and field of view. To ensure self-consistency between quantities in simulations and observations, we developed a framework to “observe” a simulation snapshot, from which we obtain “observed” structural parameters. For reference we also provide structural parameters using the usual theoretical/numerical definitions. Quantities that derive from the “observation” of a snapshot have no markings.

We adopt instead a curl-bracketing with an underscore “s” ($\{\}_s$) to denote the definition of a quantity based on current practice in numerical simulations (the “s” subscript stands for simulation).

3.1. Observation of a simulation snapshot

The positions and velocities of all particles in our simulations are saved every 10 code time units (one time unit is about one dynamic time; see Heggie & Mathieu 1986). We then proceed to construct a synthetic observation by first ignoring all particles except main sequence stars. As our simulations only have an instantaneous step of stellar evolution, we don’t consider stars along the giant branch. This choice is appropriate for comparison with star counts maps at high angular resolution, such as HST observations, because giants are typically masked out of the analysis (e.g. see De Marchi et al. 2007). Focusing on main sequence stars allows us to significantly reduce the surface brightness profile fluctuations that arise from the small number of luminous giants that would otherwise dominate the light profile.

We then select a random direction and project the main-sequence stars positions creating a 2-dimensional map. Within this map we search for the center of the system using the Casertano & Hut (1985) density-center method.

A circular surface brightness profile is then constructed using $Int[\sqrt{N_{MS}}]$ annuli (where N_{MS} is the number of main sequence stars) each containing $\sim \sqrt{N_{MS}}$ sources. From this profile we define the half-light radius in projection r_{hP} as the radius containing half of the total luminosity. The King concentration parameter $c = \log_{10}(r_t/r_c)$ is determined by fitting the surface brightness profile with a single-mass King (1966) model. We use a precomputed King profile table with uniform spacing in W_0 ($\Delta W_0 = 0.1$). The fit is carried out imposing that the total luminosity and half-light radius of the fitting model match those of the simulation snapshot within a $\leq 1\%$ deviation. From W_0 and r_{hP} we derive r_t and r_c . As an alternative definition for the observed core radius we consider the radius at which the surface brightness profile reaches half of its central value and we indicate this quantity with r_μ .

To construct the global mass function of the system, we proceed to identify close pairs of stars whose light would be blended together, similarly to the procedure described in Gill et al. (2008) and Pasquato et al. (2009). Our main aim is to treat binaries in the simulations consistently with observations. We capture also line-of-sight superpositions and therefore crowding. For reference we set an HST-like resolution of 0.05 arcsec and we consider the

system, of assumed half-light radius 3 pc, at a distance of 5 Kpc from the Sun. This implies that we consider blended those stars separated by less than 250 AU, which includes all our primordial hard binaries. In addition, we get a small number of apparent binaries, typically up to a few tens per snapshot depending on the central concentration of the system. Given a set of blended stars, we only consider the brightest member of the ensemble as observable for the purpose of re-constructing the stellar mass function. As the luminosity of a main sequence star scales approximately with $M^{7/2}$, this is an adequate approximation. With this procedure we define a catalog of observable main sequence stars where we include stars down to $0.2 M_{\odot}$ (for reference the observed mass function of NCG 2298 has greater than 50% completeness at the center at this mass limit; see Pasquato et al. 2009).

The stellar mass function in main sequence stars is modeled as a power law. Its index α is obtained by maximizing the likelihood L :

$$\log L(\alpha) = -N_{MSR} \log \left(\frac{m_u^{\alpha+1} - m_d^{\alpha+1}}{\alpha + 1} \right) + \alpha \sum_{i=1, N_{MSR}} \log(m_i), \quad (7)$$

where N_{MSR} is the number of resolved main-sequence stars and m_d and m_u are their minimum and maximum mass (here 0.2 and 0.8 M_{\odot}).

Based on the catalog of resolved main-sequence stars used above to retrieve α , we define the total observed main-sequence mass of the system M as:

$$M = \sum_{i=1, N_{MSR}} m_i. \quad (8)$$

3.2. 3-Dimensional, Mass-Based Structural parameters

In a numerical simulation code such as NBODY6, the tidal radius $\{r_t\}_s$ is defined based on Eq. 6. We define as $\{M\}_s \equiv M_T$ is the total mass of the cluster (including dark remnants such as black holes, neutron stars and white dwarfs), that is the mass of all the particles within $2 \{r_t\}_s$ from the center of the cluster.

Several different definitions have been used in numerical simulations for the core radius, so we direct the reader to Trenti, Heggie & Hut (2007) for a comprehensive discussion. Here we adopt the standard definition from Casertano & Hut (1985):

$$\{r_c\}_s = \frac{\sum_{i=1, N_{tot}} m_i r_i \rho_i}{\sum_{i=1, N_{tot}} m_i \rho_i}, \quad (9)$$

where r_i is the distance from the center of the system and the sum is made over all the N_{tot} particles of the system (including dark remnants). The density ρ_i around each particle

is computed from the distance to the fifth nearest neighbor (Casertano & Hut 1985). In passing we note that this is *not* the NBODY6 definition of $\{r_c\}_s$, which is based on a ρ_i^2 weight (see Trenti, Heggie & Hut 2007). The half-mass radius of a simulated system ($\{r_h\}_s$) is defined as the tri-dimensional radius that contains half of the total mass of the system ($\{M\}_s$), thus including again any compact remnant that does not contribute to the surface brightness profile of the system.

4. Results

4.1. Mass Function Evolution

The evolution of the mass function index α is shown in Fig. 1 as a function of the observed remaining mass of the system. As time progresses (and thus the system loses stars and mass), the mass function is preferentially depleted of low mass stars and becomes flatter (larger α). Models in a stronger external tidal field lose stars faster (Trenti, Heggie & Hut 2007) and consequently have larger variation in α . However when looked at in terms of the remaining fractional mass, the evolution of α becomes independent of the tidal field strength and almost independent of the binary fraction considered in the runs. A larger binary fraction tends to moderately slow down the flattening of the mass function because low mass stars can be retained, and observed, if they have a dark remnant as a companion. All the simulations in Fig. 1 start with the same IMF below the turn-off (but with different retention fractions of neutron stars and black holes in the right panel). In addition, their initial conditions are such that the tidal field cut-off is self-consistent with the initial density profile of the system. To investigate if a universal evolution of the mass function index is present in a broader range of conditions, we consider in Fig. 2 additional runs that either start from a different IMF (Salpeter) or that are initially underfilling their Roche lobe. For the latter, we start from a $W_0 = 3$ King model but we set $\{r_t\}_s = 6.28$, which is twice as large as the self-consistent $\{r_t\}_s (W_0 = 3) = 3.14$. To compare the evolution of different mass functions, we consider the change in the power-law fit of the mass function: $\Delta\alpha = \alpha(t) - \alpha(t = 0)$. From Fig. 2 it is immediately clear that the two simulations starting with a Salpeter IMF behave very similarly to the Miller&Scalo runs. The run initially starting with an underfilled Roche lobe does instead evolve marginally faster. $\Delta\alpha$ is in fact larger at a given fraction of mass loss, especially in the early stages of the evolution of the system. At later times the Roche lobe is eventually filled, consistent with the results of the simulations by Gieles & Baumgardt (2008). At that point the evolution of $\Delta\alpha$ is similar to our standard models. The close correlation between the slope of the stellar mass function and the fraction of the initial mass lost by a cluster was also found in previous

studies (Vesperini & Heggie 1997; Baumgardt & Makino 2003). Our simulations confirm this relation and show its validity for a broader range of different initial conditions. Recently, Kruijssen (2009) investigated the evolution of the mass function with an analytic model, that reproduces the universality of $\Delta\alpha$ for different IMF. The Kruijssen (2009) conclusion that the retention fraction of black holes influences the evolution of the mass function (see Fig. 15 and Sec. 5.2 in that paper) is however not seen in our simulations. This is likely because the analytic model of Kruijssen (2009) does not take into account multiple encounters (three body or higher) of stellar black holes that contribute to their mutual ejection on a relaxation timescale (Merritt et al. 2004). The models of Kruijssen (2009) with different retention fractions start to show differences in the evolution of α when more than half of the mass of the system is lost. At that point only a few stellar mass BH would have survived in the system, independently of their initial number (e.g. see Merritt et al. 2004; Gill et al. 2008).

The quasi-universal evolution of α as a function of $M/M(t = 0)$ is very interesting because, if the initial mass function of Galactic globular clusters is universal, as for example suggested by Kroupa (2002), then the slope of mass function is a direct tracer of the mass loss of the system, and thus of its dynamical age and of the tidal field it experienced during its life. This diagnostic is most effective to detect a large mass loss as $|d\alpha/dM|$ steepens when M decreases. Our conclusions on the quasi-universality of the α evolution can be applied to old globular clusters, with a turn-off mass below $1M_\odot$. For younger systems both the turn-off mass and the tidal disruption timescale may introduce deviations from the universal behavior observed here (Kruijssen 2009). Finally it is interesting to note that our conclusions are consistent with Galactic globular clusters observations of α (De Marchi et al. 2007): the clusters more massive than $\sim 2 \times 10^5 M_\odot$ have essentially the same α , while lower mass clusters usually show a broader range of α values, likely indicating that mass loss has taken place.

4.2. Structural parameters from King model fits

The evolution of the observed structural parameters also tends to attain a universal configuration, as shown in Figs. 3 and 4 for the core-to-half-light radius ratio and in Fig. 5 for the concentration c . The left panel of Fig. 3 shows the r_c/r_{hP} evolution of $N = 64k$ models with different tidal field configurations and initial density profiles as well as a binary fraction from 0% to 5%. Eventually all these models reach a common value for the *observed* r_c/r_{hP} ratio as derived from King profile fitting. However the observed r_c/r_{hP} ratio behaves differently from the theoretical and numerical expectation for $\{r_c/r_h\}_s$. In fact, core-collapse for systems made only of single stars is detectable only for a very short time based on

r_c/r_{hP} . After core-collapse, runs with 10% primordial binaries, (left panel of Fig. 4) behave essentially as those with single stars only. We interpret this result as a consequence of mass segregation of dark remnants at the center of the cluster. The dark-remnants are on average heavier than the main sequence stars and thus they transfer kinetic energy to them. This results in a heating of the visible component of the cluster, which therefore does not exhibit a typical core-collapsed structure. An independent confirmation of this trend can be inferred from Fig. 5 in Hurley (2007), where runs with and without primordial binaries also have a similar core (although Hurley 2007 runs do not reach past core-collapse). The core collapse for single-star systems is instead well discernible from the evolution of $\{r_c/r_h\}_s$ (see Fig. 6). Until core-collapse, theoretical and observed King-fitted core radii evolve similarly, but immediately after the core bounce the two definitions separate sharply from each other. Post core-collapsed systems develop a shallow central cusp ($\mu \sim R^{-\nu}$ with $\nu \sim 0.4 - 0.7$) that is missed by the best fitting King model (see Fig. 7), whose structure is constrained by the global surface brightness profile. In general, a King model becomes a poorer description of the system after core-collapse: in fact, the quality of our fits is degraded by about a factor two, as measured by the ratio of typical χ^2 before and after core-collapse. As a consequence, the fit results in the post core-collapsed phase also become somewhat dependent on the modeling of photometric errors. We assumed a constant fractional error on the surface brightness profile, which corresponds to a constant error in magnitude, except for the outer points, where we assigned a constant error in flux (to model the effect of the sky background). Assuming a constant error in flux for all the points in the surface brightness profile yields to no differences in the fit before core collapse. After the collapse, slightly more concentrated models are preferred, because in this case the points with the highest surface brightness have an increased weight relative to the outer points.

The results in Fig. 3 have been obtained assuming a Miller & Scalo (1979) IMF and a 100% retention of neutron stars and stellar-mass black holes. A Salpeter (1955) IMF has a higher fraction of dark remnants per unit mass (because of its shallower slope, $\alpha = -2.3$, compared to the MS IMF, $\alpha = -3.3$, in the range $[10 : 100]M_\odot$), thus it sustains a larger core, especially in the earlier stages of the simulation (see right panel of Fig. 4). This effect is primarily due to stellar mass black-holes (Merritt et al. 2004; Mackey et al. 2008), so r_c/r_{hP} returns in line with that of the Miller & Scalo (1979) simulations once the BHs segregate at the center of the cluster and kick each-other out of the system via three body interactions. Reducing the retention fraction of neutron stars and BHs to 30% leads to a decrease of the core radius down to $r_c/r_h \sim 0.05$, albeit with large fluctuations. The large fluctuations that appear after the core-collapse are also related to the degraded fit-quality, which increases the uncertainty on c (that is on W_0).

Interestingly, the main-sequence surface brightness profile has a significantly larger core

in the run with a central IMBH compared to all other runs once they reach their long-term equilibrium configuration (see right panel of Fig. 4). The prediction of Trenti et al. (2007) and Gill et al. (2008) that collisionally relaxed systems with a central IMBH should exhibit a large r_c/r_{hP} is thus confirmed (see also Baumgardt et al. 2005). However systems with a large core radius might also be in the pre-core collapse stage. Unless the cluster relaxation time is short enough to suggest the cluster should have already undergone core collapse, no IMBH (or IMBH-like heating) is required to explain large values of r_c/r_{hP} . A small value of r_c/r_{hP} , on the other hand, can be safely used to exclude likely candidates to harbor an IMBH.

Fit of the surface brightness profile with a King model does not appear to provide a very solid determination of the intrinsic tidal radius of the system. The comparison between r_t and $\{r_t\}_s$ in Fig. 8 shows that, when the entire surface brightness profile is used for the fit, then $r_t > \{r_t\}_s$. This is however not surprising, because unbound particle escaping from the system are removed from the calculation only when they have $r > 2\{r_t\}_s$, thus the surface brightness profile at radii beyond $\{r_t\}_s$ may still be positive. Similarly in actual star clusters, unbound stars remains initially in the proximity of the system, while escaping. The measure of r_t becomes more uncertain, and dependent upon the details of the fit, if only a fraction of the surface brightness profile points is used (see blue dotted line in Fig. 8). This is especially true after core-collapse (that is at $M/M(0) \lesssim 0.65$ in Fig. 8). This is primarily because we carried out the fit over the full-surface brightness profile by fixing the total luminosity and the half-light radius within 1% of the values in the profile. If only a fraction of the points is available, these two scales cannot be measured directly and must be left as free parameters of the fit. This leads to increased uncertainty, especially after core collapse, when the surface brightness profiles might present some departures from a King profile (for example see Fig. 9 at $R \sim 0.15$). When we do not use the outer points in the fit, the tidal radius tends to be moderately underestimated after core collapse compared to the determination using the full profile (Fig. 8). This is consistent with what has been found in the determination of the tidal radius for some Galactic globular clusters (McLaughling & van der Marel 2005). A different conclusion may however be reached for those globular clusters that do not fill their Roche lobe (Baumgardt et al. 2009).

4.3. Alternative core radius definitions

Given the difficulty in reliably identifying core-collapsed systems from King model fitting, we explore here alternate definitions for the observed core radius. One possibility is to use the classical core radius r_μ , that is the radius at which the surface brightness falls to

half of its central value. A comparison between r_c and r_μ is shown in Fig. 10 and suggests that this definition is better suited for identifying core-collapsed systems. r_μ remains in fact close to $\{r_c\}_s$ (within $\sim 15\%$ accuracy), confirming for complex dynamic configurations that include mass segregation the results published by Casertano & Hut (1985) for King profiles with a constant mass-to-light ratio. However the definition of r_μ depends on the choice of bins, especially on the central one. Too small a bin size will lead to large Poisson fluctuations in the central surface brightness value, while an excessively large bin will overestimate the core size by lowering the central value of the surface brightness. A large central bin is not necessarily a choice, but may be imposed in actual observations by a limited angular resolution. To overcome some limitation related to binning, Casertano & Hut (1985) proposed to extend the density-based core radius estimator to the surface brightness profile $\mu(R)$ and to define a surface-brightness density radius s_μ . In our notation this reads:

$$s_\mu = \frac{\sum_{i=1, N_{MSR}} \mu(R_i) R_i}{\sum_{i=1, N_{MSR}} \mu(R_i)}, \quad (10)$$

where the sum is carried out over all the detected main-sequence stars. s_μ is shown for our simulations in Fig. 10. As expected from Fig. 3 in Casertano & Hut (1985), s_μ deviates from r_μ and $\{r_c\}_s$ for high-concentration King models, that is mainly in the post core-collapsed phase. Interestingly the value of r_c obtained from King fitting for post core-collapsed systems is approximately bound between r_μ and s_μ .

4.4. Fluctuations

Fluctuations in the structural parameters beyond those expected from Poisson noise are clearly apparent from our analysis. Heggie & Giersz (2009) reach the same conclusion for their simulation of NGC 6397. Our run with a Miller & Scalo (1979) mass function and low retention of dark remnants has particularly strong fluctuations, as can be seen for all different core radius estimators in Fig. 10. It is very interesting to note that the system appears to go through some breathing phases, where subtle changes are made to the surface brightness profiles, affecting primarily the King model fit. The origin of these fluctuations is likely dynamical, especially because we are considering only the main-sequence stars and thus we are relatively unaffected by low-number statistics.

4.5. Identification of core-collapsed systems

Our results on the determination of core radii have profound implications for our understanding of the dynamical state of observed globular clusters: most intrinsically core-collapsed globular clusters in our simulations appears to have a surface brightness profile in main sequence stars essentially identical to non-core collapsed systems when a King model is used to retrieve r_c . Furthermore our simulations do not predict very small r_c if the retention fraction of neutron stars and black holes is high. Alternative definitions of the core radius, such as r_μ , are more efficient at identifying core-collapsed clusters, but they may still suffer from large fluctuations and/or biases due to finite resolution at the center of the system. This picture clearly illustrates the potential problems in the observational identification of core collapsed clusters. In fact, the classification of an observed globular as core-collapsed or not might be a result of the combination of significant fluctuations in the total surface brightness profiles (enhanced with respect to our main-sequence only analysis because the profile is defined primarily by a small number of giant stars; see also Heggie & Giersz 2009), combined possibly with the limited angular resolution of ground-based data (Trager et al. 1995) used to construct the structural parameters presented in the Harris (1996) catalog. The core size in the post core-collapse phase depends mildly ($\propto 1/\log(0.11N)$) on the number of particles in the system (Vesperini & Chernoff 1994; Heggie, Trenti & Hut 2006), thus it is expected that smaller core radii can be measured in systems with a larger number of particles. Further exploration of this issue is deferred to a follow-up paper that will include live stellar evolution to follow stars off the main sequence and thus to correctly model the total luminosity of the cluster. This will allow us to carry out a more direct comparison with the ground-based data that define r_c in the Harris (1996) catalog.

4.6. Evolution in the $(c; \alpha)$ plane

An interesting correlation has been recently reported by De Marchi et al. (2007) between the slope α of the global stellar mass function of globular clusters and their central concentration c . Less concentrated clusters are more depleted in low mass stars than those with higher values of c .

The evolution of a star cluster in the $(c; \alpha)$ plane is driven by collisional (two-body) processes, thus the De Marchi et al. (2007) observations test our understanding of the dynamics of globular clusters. As discussed in Sec. 1, the observed correlation appears to be in conflict with the standard scenario globular cluster evolution which predicts that relaxation drives an increase in c as the cluster evolves toward core collapse while at the same time preferentially depleting the system of low mass stars via evaporation (Spitzer 1987). The evolution

of our simulated star clusters in the concentration-slope of the mass function ($c - \alpha$) plane is shown in Fig. 11, where we also report the values observed by De Marchi et al. (2007) for those clusters that are well relaxed ($t_{rh} \leq 1$ Gyr) according to the Harris (1996) catalog. In plotting the concentration parameter c for the clusters shown in Fig. 11 we have used the values obtained by McLaughling & van der Marel (2005), which are based on the King (1966) models. Differences from the concentration values reported in De Marchi et al. (2007) are however very small ($\Delta c < 0.1$, except for NGC 6712 which has $c = 1.05$ in McLaughling & van der Marel (2005) and $c = 0.9$ in De Marchi et al. (2007)). While our simulations never reach a deep core-collapse ($c \gtrsim 2.5$), their concentration tends to evolve toward $c \sim 1.7$, still larger than what observed for the systems with the most depleted stellar mass function. One possibility to explain the system with lower concentrations remains that of a very efficient source of heating at the center of the system, comparable with the heating generated by an IMBH (see cyan line in Fig. 11). An IMBH itself appears to be excluded as the preferred explanation, because NGC 2298, where a central IMBH is rejected at high confidence level (Pasquato et al. 2009), is one of the low c points in Fig. 11. Stellar mass black-holes are also very unlikely to be viable, because the heating source needs to remain efficient in the latest stages of the evolution of the system. Stellar mass BHs lose instead efficiency at later times (see red line in the lower panels of Fig. 6; see also Merritt et al. 2004). It has been recently suggested that white dwarf kicks can sustain a large core (Fregeau et al. 2009). However the effect of the kick has been shown only at the level of $\{r_c/r_h\}_s$ and thus its full impact on the observed concentration c is an open question.

An alternative explanation for the discrepancy in the ($c; \alpha$) plane evolution might rest in observational biases. While we carried out our analysis restricting to main-sequence stars, the tidal radius of observed globular clusters is mainly derived from ground-based data (Trager et al. 1995), that thus are mostly dominated by giant-branch stars. Therefore mass segregation might lead to a systematic underestimate of r_t from these observations compared to our analysis.

Overall Fig. 11 shows that the correlation between α and c observed by De Marchi et al. (2007) is still in mild disagreement with the expectations from numerical simulations. Half of the 8 observed clusters are consistent with our models (including NGC 2298 which has ($c = 1.31; \alpha = 0.5$) and could be explained by a core fluctuation). Two of them appear instead to be core-collapsed clusters. They have a conventional concentration $c = 2.5$, higher than our what we obtain from our simulations, as discussed in Section 4.2 (but they could be explained by assuming a low retention fraction of neutron stars and black holes). Two clusters have instead concentrations below our predictions, but here the consistency of simulations and observations might improve if data and models are analyzed with a fully self-consistent approach.

5. Conclusion and Discussion

In this paper we discussed the evolution of the global mass function index α and of the structural parameters for multimass direct N-body models of star clusters in a galactic tidal field with and without primordial binaries using a total number of particles up to $N = 65536$. We adopted a Miller & Scalo (1979) initial mass function evolved with an instantaneous step of stellar evolution to a turn-off mass of $0.8 M_{\odot}$. The simulation results have been interpreted with great care in order to use definitions of structural quantities consistent with observations of Galactic star clusters.

The initial density profile of the cluster or the tidal density field is not important in the long term, as the memory of the starting concentration is erased on a relaxation timescale, with a similar subsequent evolution for models starting from different initial conditions (see figs. 1 to 5). r_c/r_{hP} appears to be stable also over different IMFs, but its value depends on the retention fraction of neutron stars and stellar mass black holes. In particular a deep core collapse can be identified from the core radius as determined following the observational procedures, r_c , only if few dark remnants are present in the system. Even a significant fraction ($f=10\%$) of primordial binaries does not appear to influence much the observational determination of the core radius. This is likely related to the heating induced by mass segregation of dark remnants in the core of the system.

These findings highlight that the core radius r_c as obtained from King model fits over the complete radial extent of the surface brightness profile are unable to reliably identify a core-collapse cluster. Post-core collapsed systems are in fact relatively well fitted by medium concentration King models, although high residuals are present at the center of the system (see Fig. 7). It is suggestive to note that these residuals appear similar to shallow cusps that have been observed in several galactic globular clusters with HST photometry (Noyola & Gebhardt 2006). In our simulations a shallow cusp ($\mu \sim R^{-\nu}$ with $\nu \sim 0.4 - 0.7$) in the surface brightness profile appears after core collapse (see Fig. 7). The presence of such cusps may thus provide a hint that a system is past core-collapse, but other indicators are needed. One possibility if high angular resolution data are available, is to use r_{μ} as a measure of the core, that is the radius at which the surface brightness falls to half of its central value. r_{μ} does in fact track the evolution of the tri-dimensional core radius defined in simulations, i.e. $\{r_c\}_s$ (see Fig. 10). In alternative, one could explore the use of the mass-to-light ratio if spectroscopic information are available. Shallow cusps at the center of medium concentration surface brightness profiles appears to be so common in the post core-collapsed evolution of a globular cluster that this indicator is not particularly helpful in suggesting clusters likely to harbor a central IMBH, contrary to past suggestions (Baumgardt et al. 2005; Miocchi 2007).

Our investigation on the evolution of structural parameters “observed” from simulations

shows an improved agreement with the $c-\alpha$ correlation identified by De Marchi et al. (2007) for Galactic globular clusters, but still the simulated clusters are too concentrated in their final stages of their evolution. This might be related to the definition of the tidal radius r_t , and thus of the concentration, from the $\gtrsim 15$ years old, ground-based data used by Trager et al. (1995). The light profile is in fact dominated by contributions from stars along the giant branch, more massive than average, and therefore more mass-segregated than the main-sequence stars we used in this analysis. In any case, from the observed $c-\alpha$ correlation we can expect, based on our analysis, that some of the systems with the most depleted stellar mass function can indeed be core-collapsed systems lurking in the sample of objects fitted by regular King profiles. This highlights the importance of carrying out a uniform survey to construct the structural parameters of Milky Way globular clusters, combining large area coverage with the high angular-resolution data at the center, like those obtained for about 50 globulars by Sarajedini et al. (2007) with HST.

We thank Douglas Heggie and the referee for useful suggestions. We are grateful to Sverre Aarseth for his dedication to constantly improving its NBODY6 code and for making every improvement publicly available. We also thank Keigo Nitadori for the development of the CUDA/OpenMP extension of the code. MT and EV acknowledge partial support from NASA ATFP grants NNX08AH29G, NNX08AH15G and from grant HST-AR-11284, provided by NASA through a grant from STScI, which is operated by AURA, Inc., under NASA contract NAS 5-26555. All the authors acknowledge support from the Kavli Institute for Theoretical Physics, through the National Science Foundation grant PHY05-51164. This research was supported in part by the National Science Foundation through TeraGrid resources provided by the National Center for Supercomputing Applications (grants TG-AST090045 and TG-AST090094).

REFERENCES

- Albrow M. D., Gilliland R. L., Brown T. M., Edmonds P. D., Guhathakurta P., Sarajedini A., 2001, *ApJ*, 559, 1060
- Aarseth S., 2003, *Gravitational N-body Simulations*. Cambridge University Press
- Baumgardt H., 2001, *MNRAS*, 325, 1323
- Baumgardt H. and Makino J. 2003, *MNRAS*, 340, 227
- Baumgardt H., Makino J. and Ebisuzaki T. 2004, *ApJ*, 613, 1133

- Baumgardt H., Makino J. and Hut, P. 2005, ApJ, 620, 238
- Baumgardt H., De Marchi, G., Kroupa, P., 2008, ApJ, 685, 257
- Baumgardt H., Parmentier, G., Gieles, M. and Vesperini, E. 2009, MNRAS, in press, arXiv:0909.5696
- Bedin, L. R., Piotto, G., Anderson, J., Cassisi, S., King, I. R., Momany, Y., Carraro, G. 2004, ApJ, 605, L125
- Belczynski K. et al. 2006, ApJ, 648, 1110
- Carretta E. et al., 2009, A&A, in press (arXiv:0909.2938)
- Casertano S., Hut P., 1985, ApJ, 298, 80
- Chernoff, D. F. and Weinberg, M. D. 1990, ApJ, 351, 121
- Davis, D. S. et al. 2008, AJ, 135, 2155
- De Marchi G. & Pulone L. 2007, A&A, 467, 107
- Demarchi, G. and Paresce, F. and Pulone, L. 2007, ApJ, 656, 65
- D’Ercole A., Vesperini E., D’Antona F., McMillan, S.L.W., Recchi, S., 2008, MNRAS, 391, 825
- Djorgovski, S. 1993, Astronomical Society of the Pacific Conference Series, 50, 373
- Fregeau, J. M. and Rasio, F. A. 2007, ApJ, 658, 1047
- Fregeau, J. M., Richer, H. B., Rasio, F. A., Hurley, J. R. 2009, ApJ, 695, 20
- Gao B., Goodman J., Cohn H., Murphy B., 1991, ApJ, 370, 567
- Gratton, R., Sneden, C., & Carretta, E. 2004, ARA&A, 42, 385
- Harris, W. E., 1996, AJ, 112, 1487
- Heggie, D. C. 1975, MNRAS, 173, 729
- Heggie D. C., Aarseth S. J., 1992, MNRAS, 257, 513
- Heggie D. C., Hut P., 2003, *The Gravitational Million-Body Problem*, Cambridge, Cambridge University Press

- Heggie D. C., Mathieu, R. D. 1986, in ‘The Use of Supercomputers in Stellar Dynamics’,
Lecture Notes in Physics, 267, 233, Berlin Springer Verlag.
- Heggie D.C., Trenti M., Hut P., 2006, MNRAS, 368, 677
- Heggie D. C. & Giersz M. 2009, MNRAS, 397, 46
- Hurley J. et al. 2000, MNRAS, 315, 543
- Hurley, J. 2007, MNRAS, 379, 93
- Hut, P. 2006, astro-ph/0601232
- Gieles, M. and Baumgardt, H. (2008), MNRAS, 389, 28
- Gill, M. et al. 2008, ApJ, 686, 303
- King, I. 1966, AJ, 71, 64
- Kroupa, P., 2002, Science, 295, 82
- Kruijssen, J. M. D. 2009, A&A, in press, arXiv:0910.4579
- Lynden-Bell R and Wood, R. 1968, MNRAS, 138, 495
- Mackey A. D., Wilkinson M. I., Davies M. B. and Gilmore G. F. 2008, MNRAS, 386, 65
- McLaughlin, D. E. and van der Marel, R. P. 2005, ApJS, 161, 304
- McMillan S., Hut P., Makino J., 1990, ApJ, 362, 522
- McMillan S., Hut P., Makino J., 1991, ApJ, 372, 111
- Merritt, D., Piatek, S., Portegies Zwart S. and Hensendorff M. 2004, ApJ, 608, 25
- Miller, G. E. and Scalo J. E. 1979, ApJS, 41, 513
- Miocchi, P. 2007, MNRAS, 381, 103
- Noyola, E. and Gebhardt, K. 2006, AJ, 132, 447
- Pasquato, M. et al. 2008, ApJ, 699, 1511
- Piotto P. et al. 2005, ApJ, 621, 777
- Piotto P. et al. 2007, ApJ, 661, 53

- Pulone L., De Marchi G., Covino S., Paresce F., 2003, *A&A*, 399, 121
- Rubenstein E. P., Bailyn C. D., 1997, *ApJ*, 474, 701
- Salpeter, E E. 1955, *ApJ*, 121, 161
- Sarajedini A. et al. 2007, *AJ*, 133, 1658
- Shara, M. M. and Hurley, J. R. 2006, *ApJ*, 646, 464
- Spitzer L., Jr, 1987, *Dynamical evolution of globular clusters*, (Princeton University Press: Princeton
- Trager, S. C., King, I. R. & Djorgovski, S. 1995, *AJ*, 109, 218
- Trenti M., Heggie D.C. and Hut P., 2007, *MNRAS*, 374, 344
- Trenti M. and Ardi, E. and Mineshige, S. and Hut, P. 2007, *MNRAS*, 374, 857
- Trenti M. et al. 2008, *MNRAS*, 387, 815
- Vesperini E., Chernoff D. F., 1994, *ApJ*, 431, 231
- Vesperini E., Heggie D. C., 1997, *MNRAS*289, 898
- Vesperini E., McMillan, S.L.W, Portegies Zwart, S., 2009, *ApJ*, 698, 615

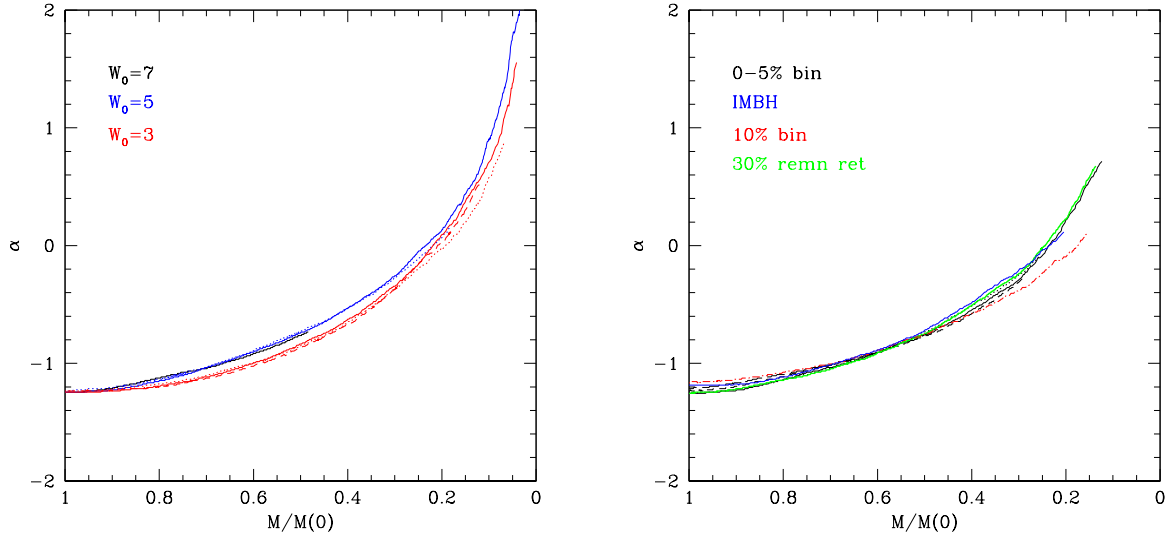


Fig. 1.— Time evolution of the mass function index α for Miller & Scalo (1979) runs as a function of the total observable mass remaining in the system M . Left panel: models with $N_{tot} = 65536$ with different tidal fields and initial density profiles (King models with $W_0 = 3, 5, 7$ — red, blue, black colors) and 0,2,5 % primordial binaries (solid, dotted, dashed lines). Right panel: $W_0 = 7$ King models starting with $N_{tot} = 32768$ particles and a binary fraction up to 10%. Black lines are a binary fraction 0-5%, the red line has $f=10\%$. A model with no primordial binaries and a central IMBH is also shown in this panel (blue). The green line shows the model with 30% retention fraction of neutron stars and black holes. The evolution of the mass function slope is almost universal.

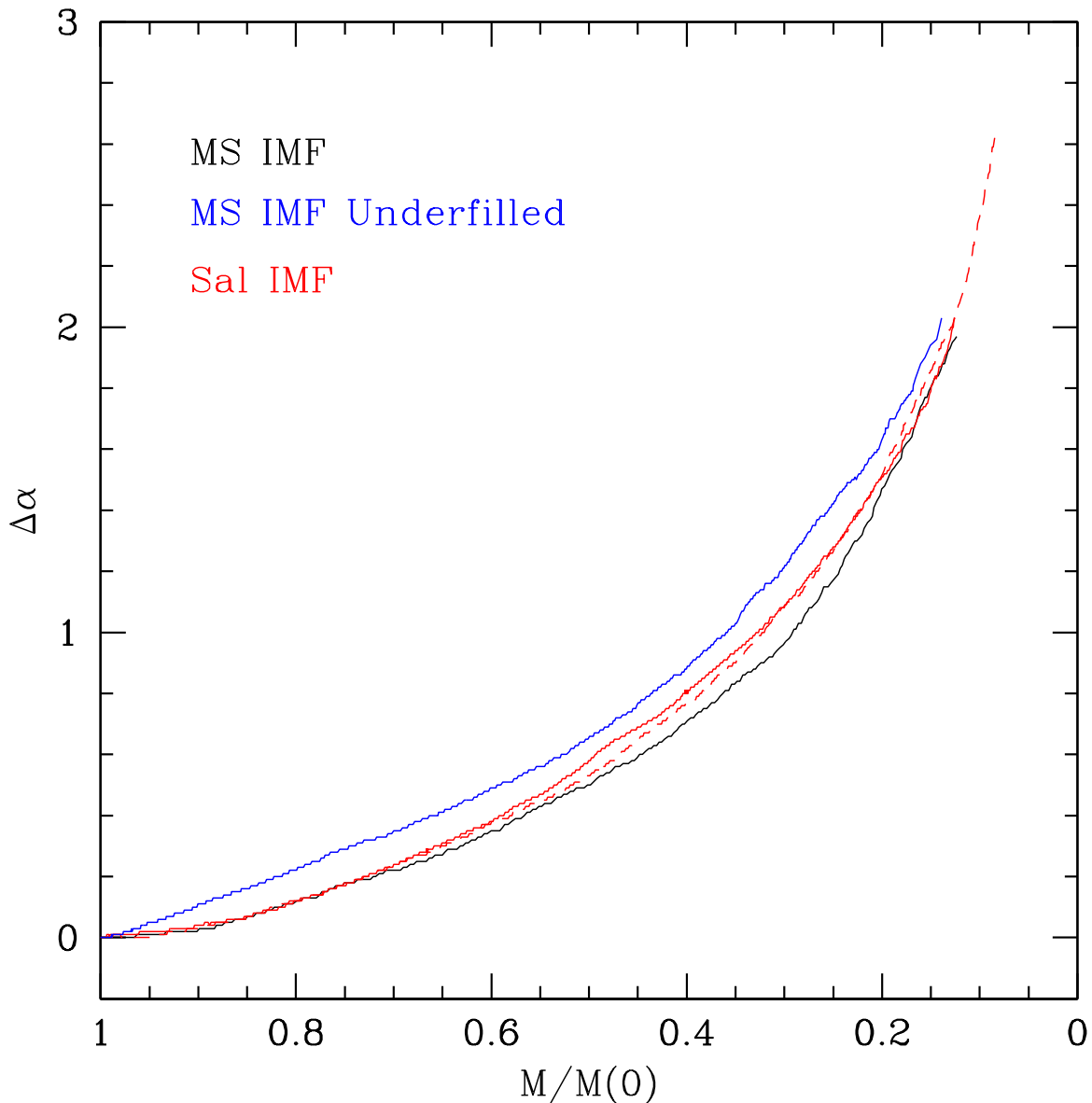


Fig. 2.— Time evolution of the mass function index α , shown as the difference from its $t = 0$ value, $\Delta\alpha = \alpha(t) - \alpha(t = 0)$, for a series of runs with a Miller & Scalo and a Salpeter mass function. The black line refers to a Miller & Scalo run with 100% retention fraction of dark remnants and no binaries starting from $W_0 = 7$. The blue line has the same IMF but starts a $W_0 = 3$ King model and $\{r_t\}_s = 6.28$ (this model has its Roche lobe underfilled by a factor 2). The red lines are runs with a Salpeter IMF, starting from $W_0 = 7$ and no binaries: (solid: 100% retention fraction, dashed: 30% retention fraction). All simulations have $N_{tot} = 32768$.

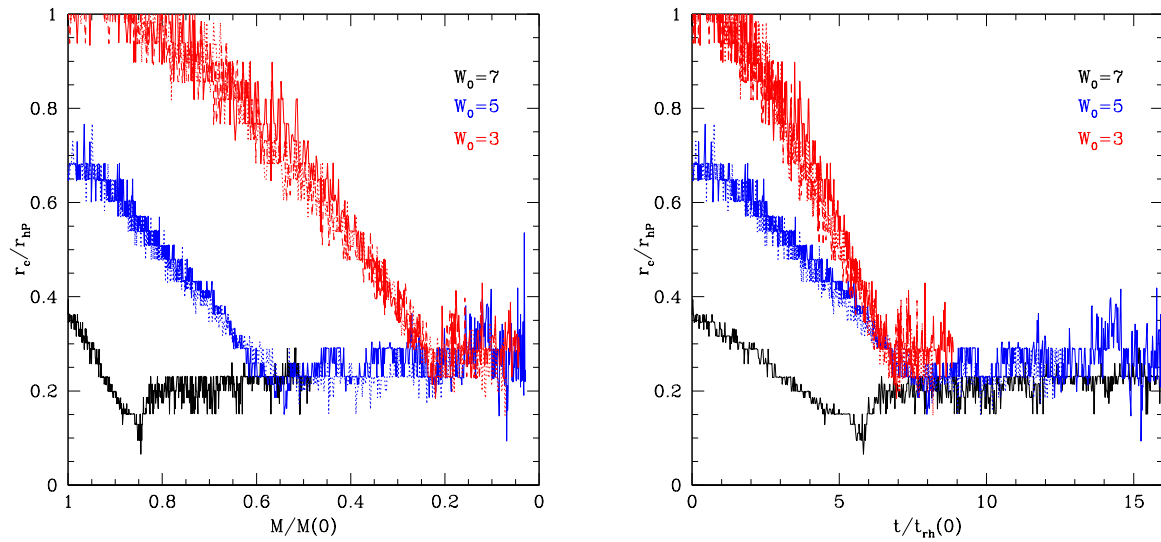


Fig. 3.— Evolution of the observed core to half light radius for our $N = 64k$ runs, color codes like in the left panel of Fig. 1. Left panel shows r_c/r_{hp} as a function of M , right panel as a function of t in units of the initial half-light relaxation time.

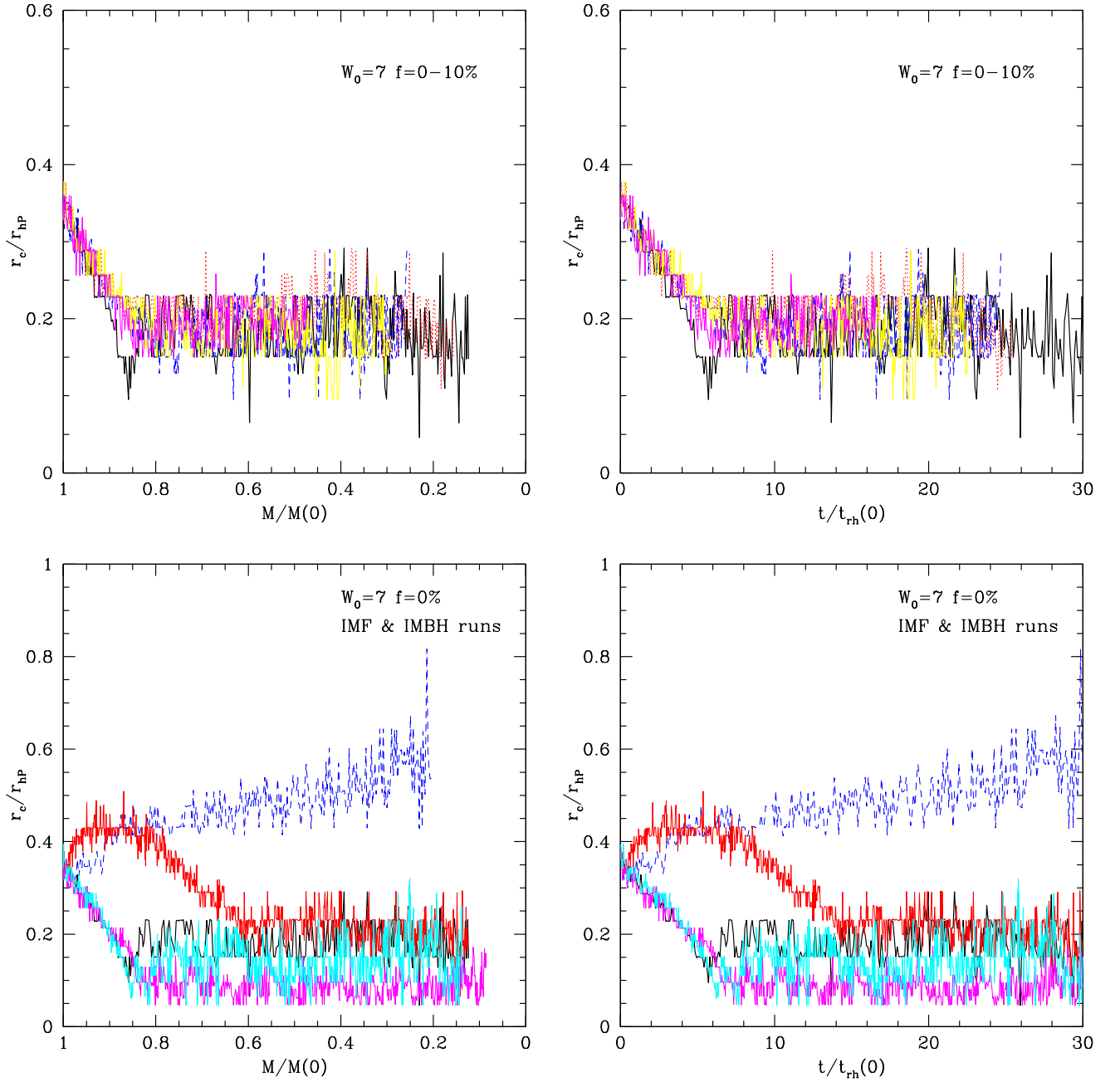


Fig. 4.— Evolution of r_c/r_{hp} like in Fig. 3 but for models with $N = 32k$. Upper set: Miller & Scalo (1979) IMF and different binary fractions (0% black, 1% blue, 3% yellow, 5% magenta, 10% red). Lower set: models with no binaries but different IMFs. Black line: Miller & Scalo (1979) with full retention of remnants, red line Salpeter (1955) with full retention of remnants. Cyan and magenta lines are the corresponding IMFs with 30% retention fraction. Blue is our run with a central IMBH. Only a central IMBH is able to sustain a large r_c in the long term, but a significant number of stellar-mass BHs can also give a transient high value of r_c . Small r_c values are instead possible with a low retention fraction of dark remnants.

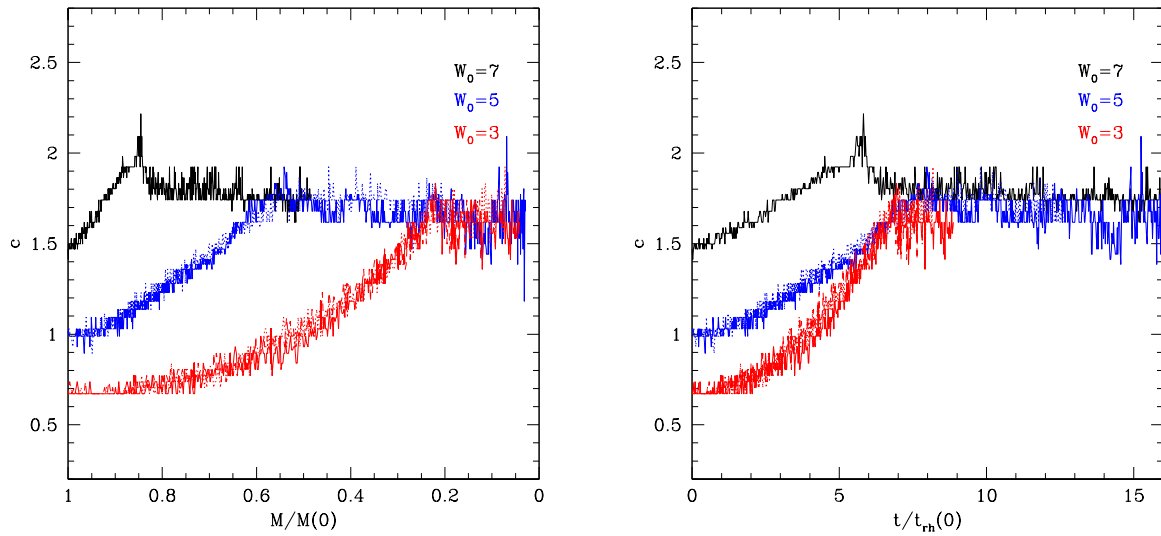


Fig. 5.— Evolution of the observed concentration c for our $N = 64k$ runs, color codes like in Fig. 1. Left panel shows c as a function of M , right panel as a function of t in units of the initial half-light relaxation time.

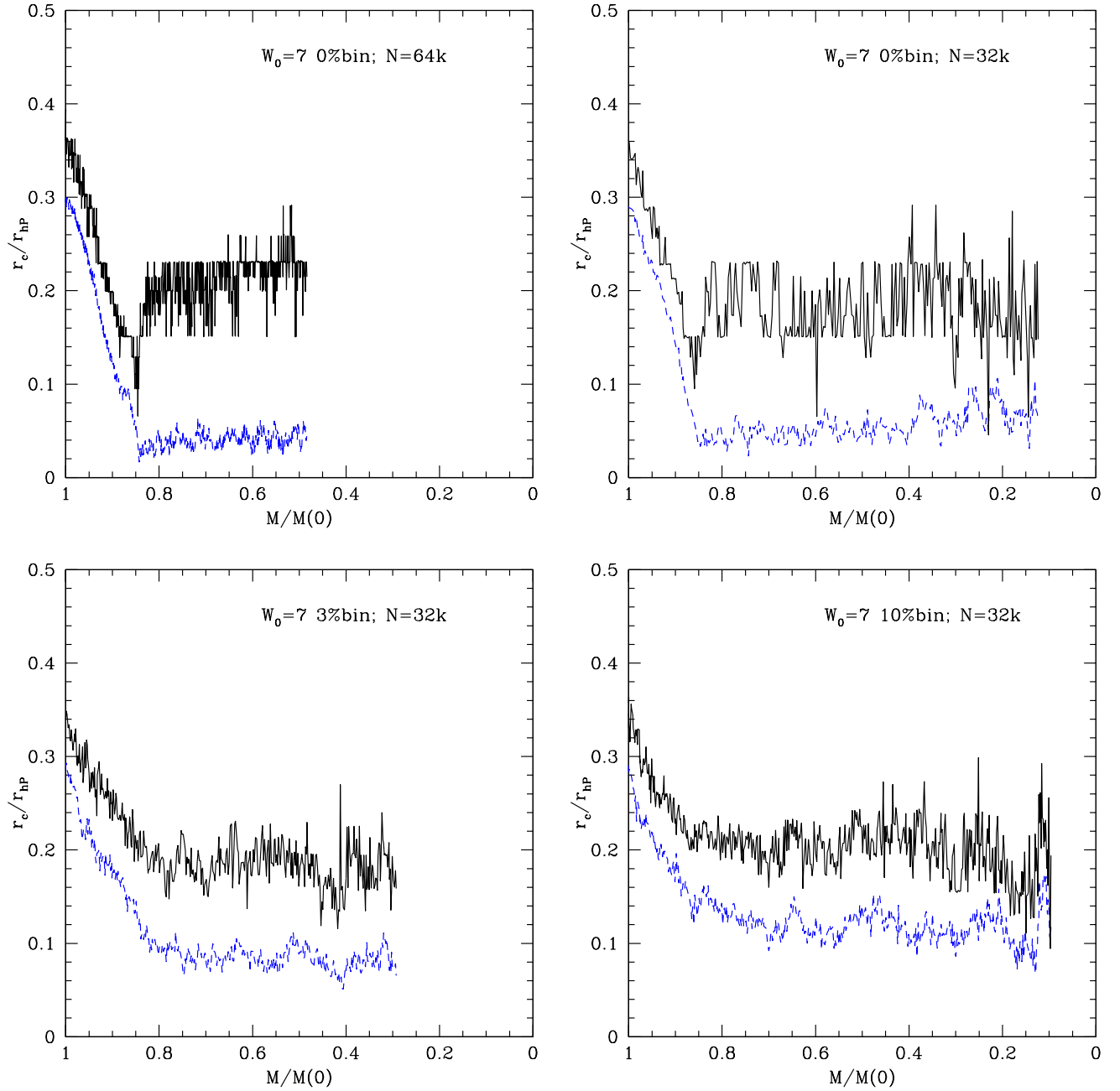


Fig. 6.— Observed core to half-light radius ratio (r_c/r_{hP} solid black line) and 3D-density based core to half-mass radius ratio ($\{r_c/r_h\}_s$ dashed blue line) for a $W_0 = 7$ model without primordial binaries ($N=64k$, upper left and $N=32k$, upper right) as well as with 3% binaries ($N=32k$, bottom left) and with 10% binaries ($N=32k$, bottom right). The two definitions differ significantly after core collapse, especially for models with a low fraction of primordial binaries. Core collapse signatures are clearly present in $\{r_c/r_h\}_s$ for models without binaries but not in r_c/r_{hP} .

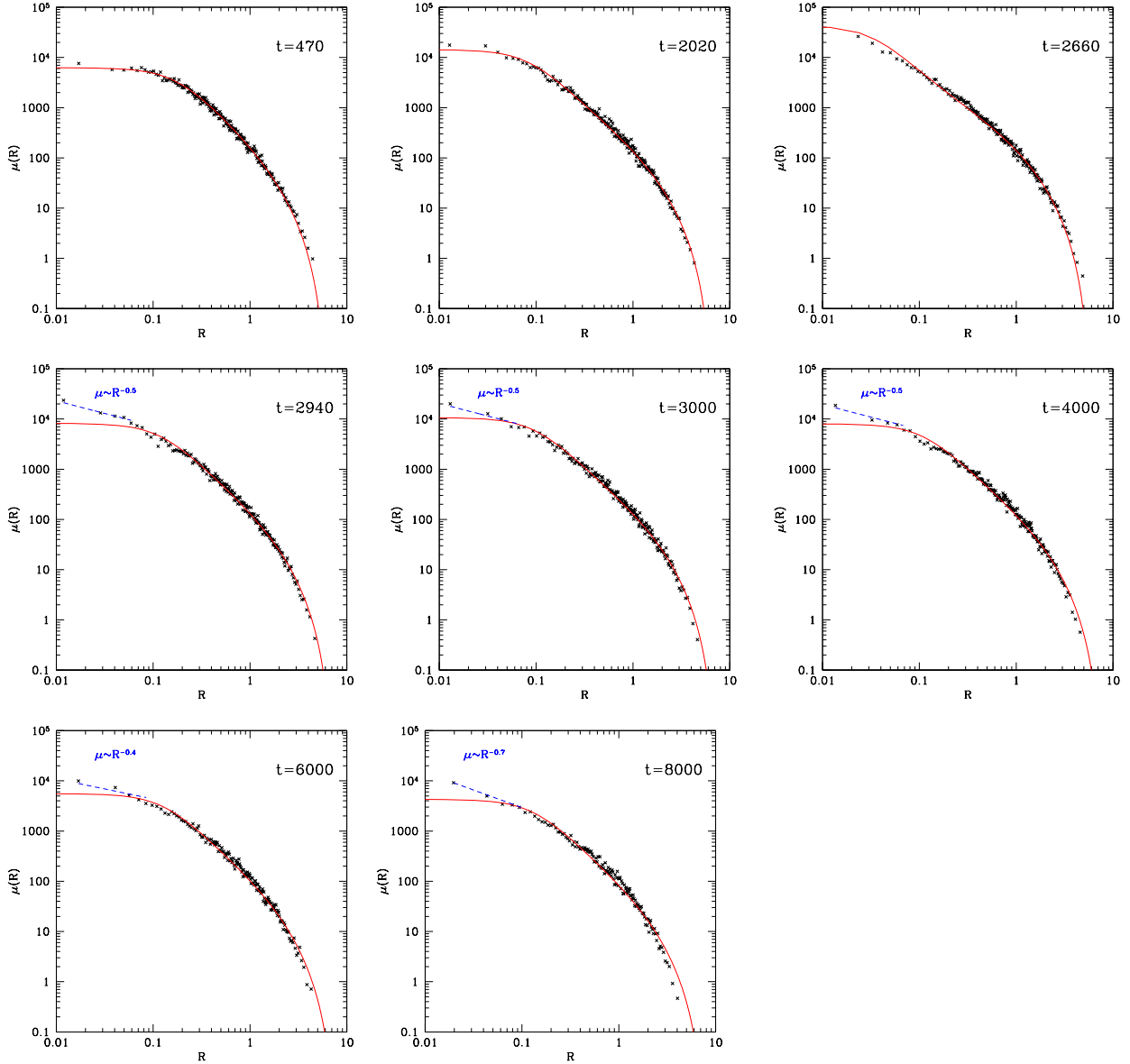


Fig. 7.— Surface brightness profiles (arbitrary units for μ , NBODY units for R) for eight snapshots of our $N = 64k$, $W_0 = 7$ simulation with no binaries. The snapshots are taken at times $t = 470, 2020, 2660, 2940, 3000, 4000, 6000, 8000$ in code units (equivalent to $\sim 1.0, 4.4, 5.8, 6.4, 6.5, 8.7, 13.1, 17.4 t_{rh}(0)$) and represents a typical pre-core-collapse profile, a profile on the way to core-collapse, the profile at the peak of core-collapse and five post-core-collapsed profiles. Superimposed to the data (black crosses) the best fit King model is shown. The five models have $W_0 = 7, 8.1, 9.4, 7.7, 8.0, 7.9, 7.7, 7.7$. The quality of the fit in the post-core-collapse profile is about two times worse than in the other snapshots. In the post-core collapse profiles (last five panels) a shallow central cusp ($\mu \sim R^{-\nu}$ with $\nu \sim 0.4 - 0.7$) is present (blue dashed line).

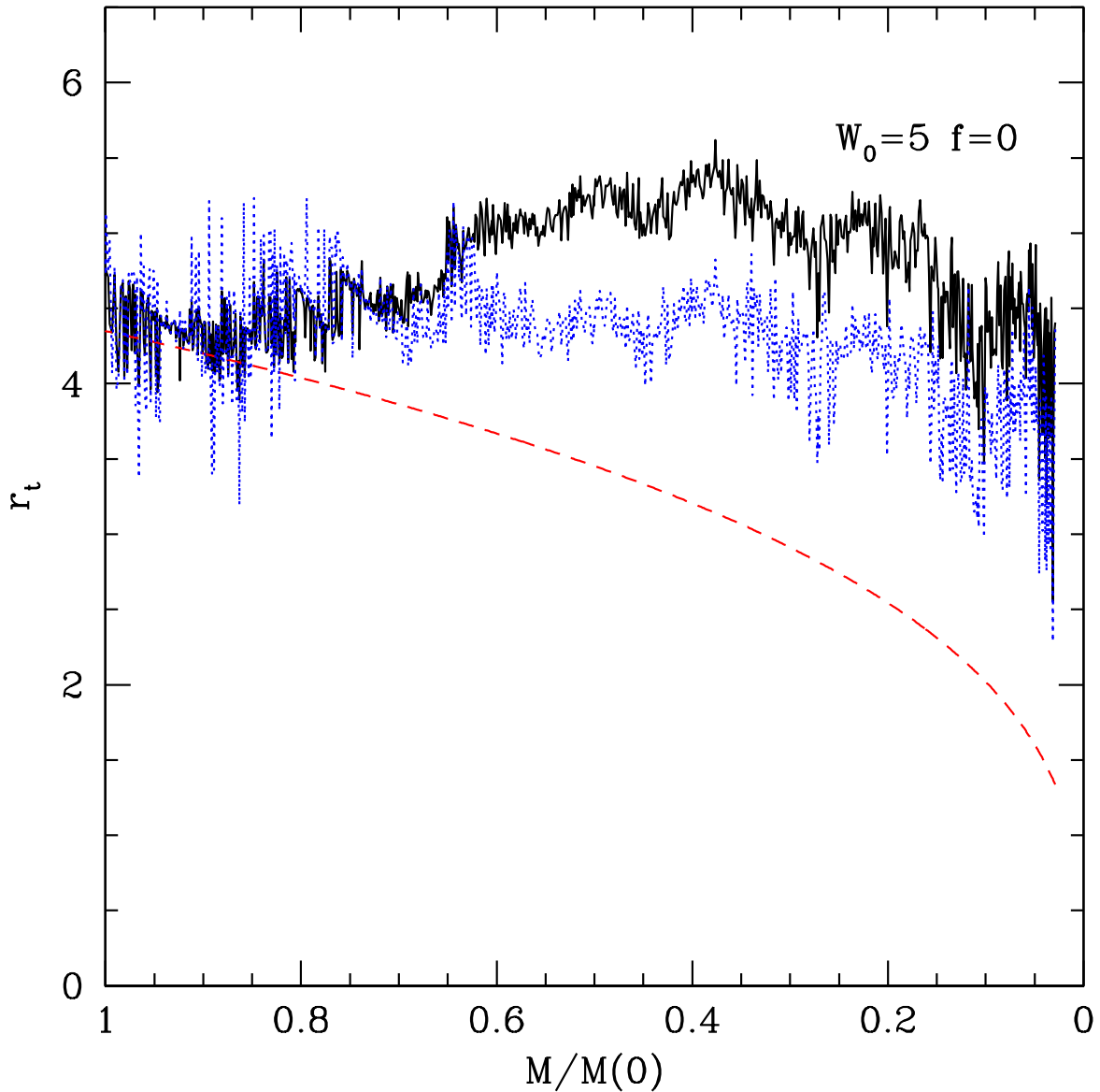


Fig. 8.— Tidal radius as measured observationally using the full surface brightness profile (r_t — solid black line) or only the inner part containing 75% of the total light (dotted blue line) in our $N=64k$ $W_0 = 5$ simulation with no primordial binaries. If information on the outer parts of the system is missing, then the tidal radius determination becomes dependent upon the details of the fitting method after core-collapse ($M/M(0) \lesssim 0.65$). The theoretical tidal radius is also shown ($\{r_t\}_s$ — red dashed line). At later times $r_t/\{r_t\}_s \sim 2$ when using the full surface brightness profile for the King model fit.

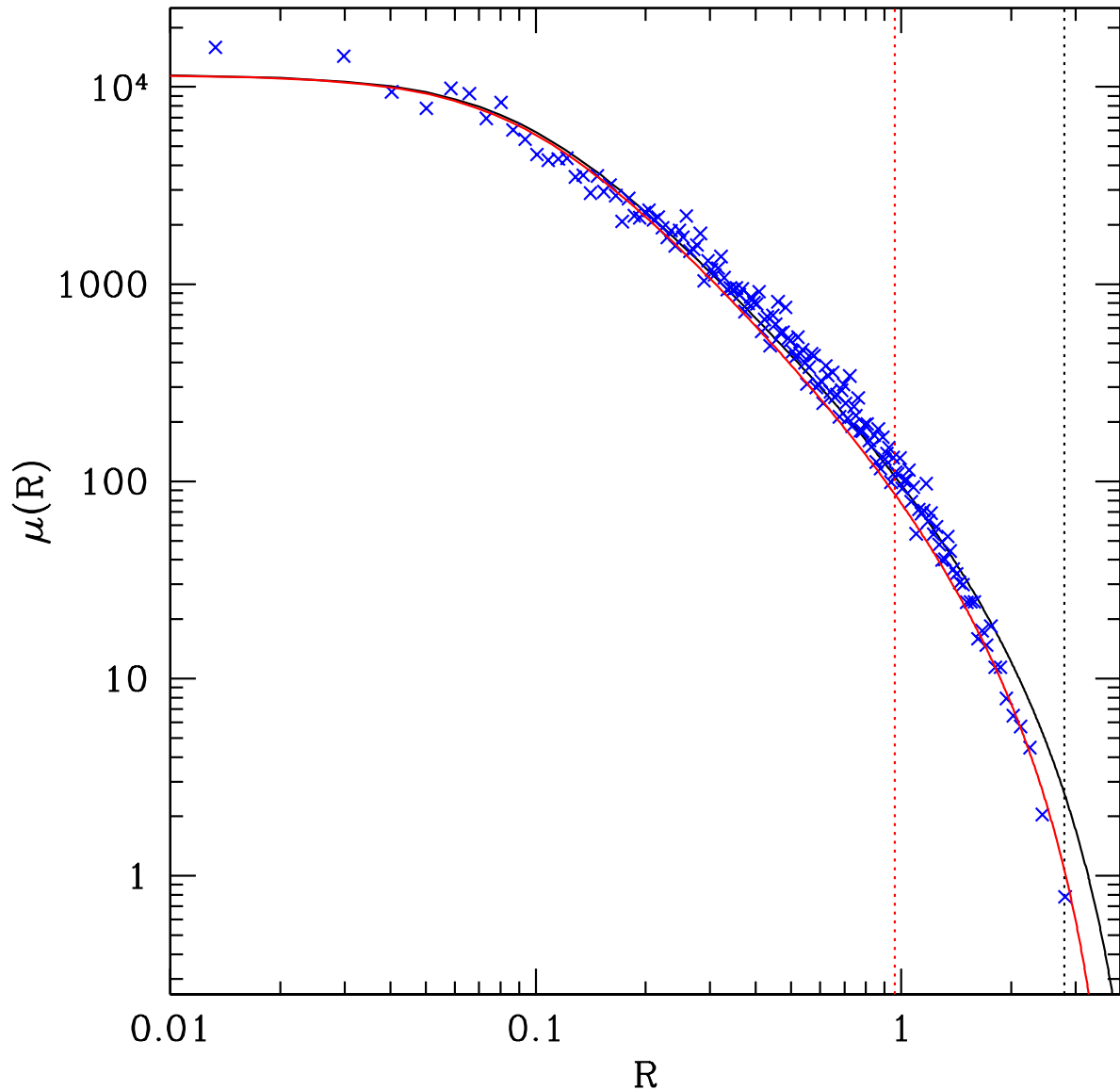


Fig. 9.— Surface brightness profile (blue crosses) at $t=3420$ (in the post-core collapse phase) for $N = 64k$ simulation with no primordial binaries starting from $W_0 = 5$. The standard King model fit over the full radial range of the profile, and with total luminosity and half-light radius fixed to the measured quantities, is shown as black solid line ($W_0 = 7.5$). A King profile fit using only the inner 75% of surface brightness profile points and with free total luminosity and half-light radius is shown as red solid line ($W_0 = 7.3$). The dotted vertical lines (black and red) show the outer boundary of the region used for fitting the King models in the first and second case.

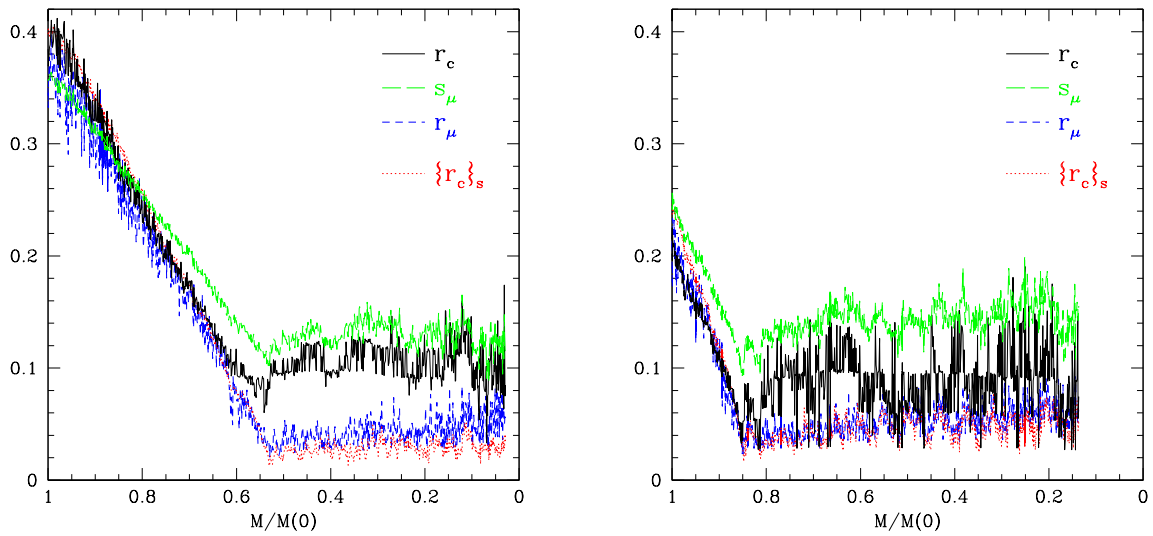


Fig. 10.— Comparison of different core radii definitions for two of our simulations without primordial binaries (left panel, $N=64k$, $W_0 = 5$; right panel $N=32k$, $W_0 = 7$, retention fraction 30%). Post core-collapse oscillations in r_c are particularly strong in the right panel.

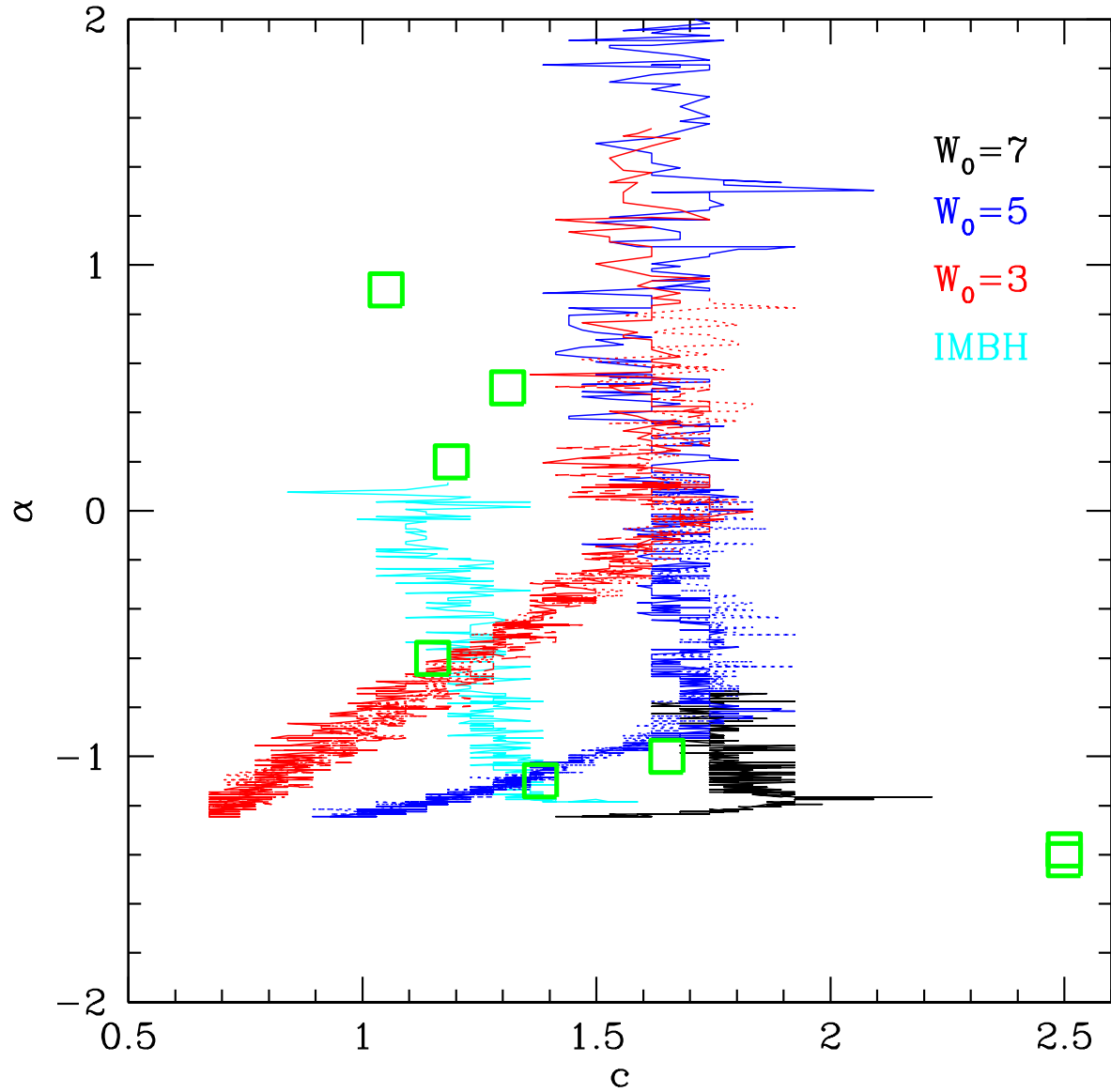


Fig. 11.— Mass function index α versus the central concentration for the $N = 64k$ models of fig. 1 and for the $N = 32k$ model with a central IMBH (cyan solid line). The green squares are points from De Marchi et al. (2007) associated to globular clusters with $t_{rh} \leq 1$ Gyr.

Table 1: Summary of N-body simulations

N	f	IMF	W_0	Other
65536	0.00	MS	3	
65536	0.02	MS	3	
65536	0.055	MS	3	
65536	0.00	MS	5	
65536	0.02	MS	5	
65536	0.00	MS	7	
32768	0.00	MS	7	
32768	0.01	MS	7	
32768	0.03	MS	7	
32768	0.05	MS	7	
32768	0.10	MS	7	
32768	0.00	Sa	7	
32768	0.00	MS	7	30% NS/BH retention
32768	0.00	Sa	7	30% NS/BH retention
32769	0.00	MS	7	$m_{IMBH} = 0.01$
32769	0.00	MS	3	$\{r_t\}_s = 6.28$ [underfilled 2]

Note. — N-body simulations of star clusters in a tidal field with self consistent King model initial conditions. First column: number of particles N ; second column: binary fraction $f = N_b/N$; third column: initial mass function used (Sa: power law, MS: Miller & Scalo); fourth column: initial concentration of the density profile (King index W_0). Fifth column reports other relevant information for the simulation. The last simulation starts from compact initial conditions where the Roche lobe is underfilled by a factor 2.